ENHANCING BUILDING RECONSTRUCTION BY ADAPTIVE FILTERING OF INTERFEROMETRIC PHASES

Clémence Dubois[(1)], Antje Thiele[(1,2)], Erich Cadario[(2)], Stefan Hinz[(1)]

[(1)]Institute of Photogrammetry and Remote Sensing (IPF), Karlsruhe Institute of Technology (KIT), Englerstr.7, 76128 Karlsruhe, Germany, Email:{antje.thiele;stefan.hinz}@kit.edu, clemence.dubois@student.kit.edu
[(2)]Fraunhofer IOSB, Fraunhofer Institute of Optronics, System Technologies and Image Exploitation, Gutleuthausstr.1, 76275 Ettlingen, Germany, Email:{antje.thiele;erich.cadario}@iosb.fraunhofer.de

ABSTRACT

The new generation of space borne sensors like TerraSAR-X and TanDEM-X is very attractive for 3D information extraction because of their high resolution and their possibility to achieve repeat-pass and since short single-pass data. Moreover, they can cover a huge area and especially their interferometric constellations allow recovering the height of objects like buildings. Nevertheless, the detection of buildings in interferometric phase data turns out to be difficult because of the high interferometric phase noise. In this paper, the focus is put on filtering the phase image at building location to enhance the building reconstruction. Different filtering methods are investigated, from the standard area filters to orientation filters, relying only on the image statistics or taking into account GIS information. These specialized filters are tested on real single-pass airborne InSAR data and compared to standard filtering methods.

1. INTRODUCTION

1.1. Motivation

The successful launch of the new satellite TanDEM-X on June 2010 opens up new perspectives for 3D mapping of the earth surface. Both high resolution and high coherence of this system support detailed 3D reconstruction of cartographic features, most prominently in urban areas. For example, the 3D reconstruction of a building can be used for supporting the planning of energy supply of built-up areas, whereby building specific volumes have to be estimated for the evaluation of the energy amount. Another application can be found in the management of crisis situations (e.g. after natural disasters like flooding or earthquakes), in which the identification of changes in the building signatures may deliver important cues for rescuers. Active SAR systems are highly attractive for this application due to their daytime and weather independency.
The work presented in the following has to be seen in the context of the building extraction approach of [1]. By use of the building footprint, an initial building height and some sensor parameters, its phase signature can be simulated. An iterative process enables to update the building height by comparing real and simulated phase signatures. An important step of this procedure is the mutual assessment of simulated and extracted interferometric phases by correlation techniques, which may suffer from the considerable noise present in the real phase image. Hence, we focus now on an adapted filtering of the interferometric phases for enhancing the building reconstruction.

1.2. Related Work

The InSAR filters proposed in the literature can be separated into two main groups: area and orientation filters. Some of the area filters investigate the frequency domain in image patches ([2] and [3]), whereas other ones like [4] are based on non-local de-noising, considering the radiometric neighbourhood of pixels instead of their spatial neighbourhood. Improvements of conventional Multilook-filtering [5] are described in [6] to increase smoothing while avoiding the elimination of significant local features. In [7], a filtering in the wavelet domain is proposed, which enables a high computational efficiency because the filtering is directly performed on the full image. Asymmetric masks were first proposed by [8] and [9], defined by a statistical analysis and region growing in the amplitude image. First orientation filters were proposed in [10], where sixteen orientation masks are considered. The orientation mask with the minimal variance of the phase values is chosen for the filtering. A similar approach is given in [11] by extending the number of orientation masks. Another technique was presented in [12], where morphological operators defined by the direction of the local gradient are used.

2. METHODS OF INSAR PHASE FILTERING

The standard filters as well as our adapted and new filters can be subdivided into three different groups characterized by the chosen type of filter window and by the introduction of prior information, and are listed in Fig. 1.

2.1. Area Filters

The first group contains the area filters that can be separated into two subgroups: those applied on the complex data and those applied directly on the phase data. For the first ones, filters 2 and 4 in the frequency domain

Proc. 'Fringe 2011 Workshop', Frascati, Italy,
19–23 September 2011 (ESA SP-697, January 2012)

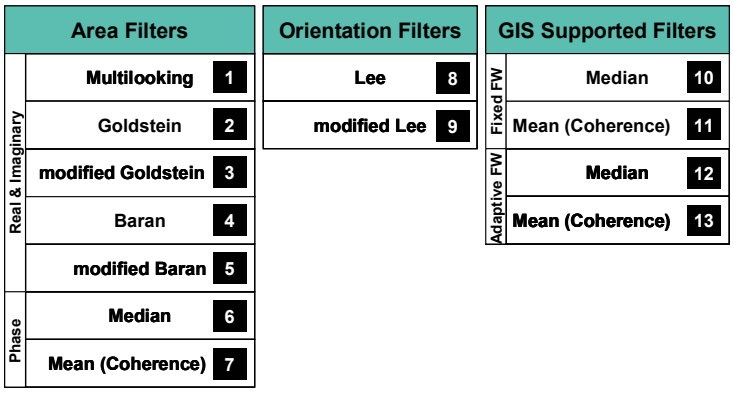

Figure 1. Investigated filters

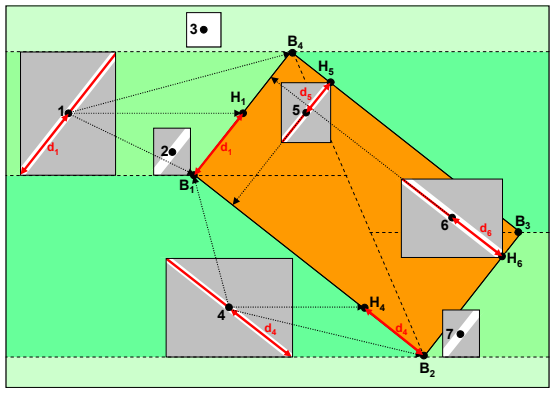

Figure 2. Schematic description of the adaptive GIS Supported Filters

([2] and [3]) have been implemented in addition to the traditional Multilook-filtering 1 (complex averaging of neighbour pixels, [5]). Modifications were made for both of them, whereby the amplitude of the frequency spectrum of each interferogram patch is smoothed with a Gaussian function (3 and 5) instead of a 3 x 3 Mean-filter. Therefore, the high frequencies corresponding to noisy values are more smoothed as the low frequencies, corresponding to less noisy pixels. For the second sub-group, a Medianfilter 6 and a coherence weighted Meanfilter 7 have been used in the spatial domain. The advantage of this last one is that the weight of each phase value depends on its coherence and so on its noise level. Thus, noisy pixels obtain small weights and have less impact on the filter result.
The main problem of these area filters is that the orientation of a building is not taken into account, which could lead to blurred results at building edges.

2.2. Orientation Filters

The second group utilizes filter masks of different orientations to enable an adaptive filtering depending on the local information. Beside the standard Lee-Filter 8 [10], a modified Lee-Filter 9 has been implemented. For this new one, the direction of the gradient is determined with Sobel within a 9 x 9 pixel window. The edge direction is assumed to be the perpendicular direction to those of the gradient. The oriented mask corresponding to the calculated edge direction is then chosen for the filtering.
Most advantage of these filters is that the building orientation is taken into account without using additional information. Only the local statistic is analyzed. However, in very noisy regions, these filters fail in finding the correct edge direction. Therefore, new filters are proposed in the following, based on integration of GIS information, for example the building footprints.

2.3. GIS Supported Filters

The third group, the GIS Supported Filters can also be separated into two subgroups. For the first (10 and 11), the same fixed oriented masks as for Orientation Filters are used. In contrast to them, the determination of the final orientation is not based on the local statistic but is defined by building edges extracted from GIS information. For the second (12 and 13), adaptive window filters are defined individual for each pixel. For these GIS-information related filters, median searching and coherence weighted averaging are implemented.
The parameterization of the adaptive filter window is visualised in Fig. 2. Considering a single building (defined by its corner points B_1, B_2, B_3, B_4) the surrounding and the building are divided in three zones (dashed lines and different green colours), where different adaptive filter windows are applied. For the external areas, which do not contain the building, (example point 3) only a 5 x 5 square window is used. For the other areas, an adaptive window is defined for each pixel, taking into account its position regarding the nearest rangeline (horizontal dashed line through each corner point) and building edge. For example, the orientation of the filter window of point 4 (considered pixels white marked) depends on the orientation of its closest building side (B_1B_2). Its size is defined employing the auxiliary point H_4, intersection of the building edge and of the translation of the pixel position in range direction. The double distance d_4 from H_4 to the nearest building corner (here B_4) corresponds to the length of its filter diagonal. For pixels inside the building footprint, the orthogonal distance to the opposite building side is used. For example, for point 6, its distance d_6 to the building edge B_2B_3 is doubled. For points, which are located exactly in the middle between two rangelines, the entire building length is considered for filtering (e.g., point 1). The closer the points are to the rangelines, the smaller are the filtering windows (e.g., point 2 and 7).

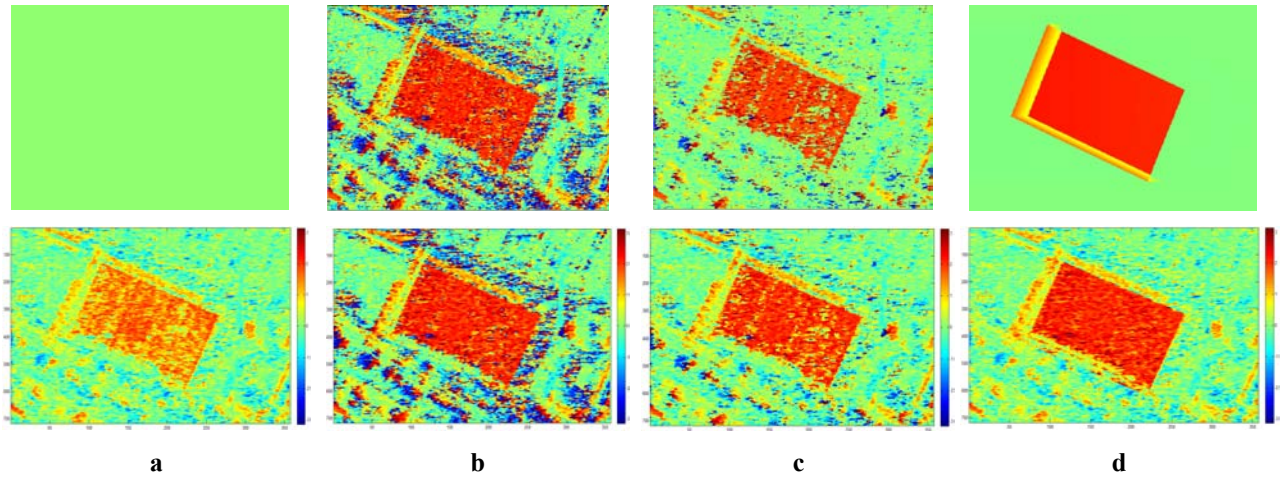

Figure 3. Unwrapping methods: offset images (upper row) and corresponding filtered phases images (lower row) for a 5x5 coherence weighted mean filter; a) no unwrapping, b) complex averaging, c) histogram analysis, d) simulated phases

2.4. Unwrapping Strategies

In [11], the necessity of local phase unwrapping was pointed out since phase filtering is not performed on complex InSAR data. For reducing observed phase underestimation, three different solutions of phase unwrapping were tested.

1. The complex mean value in a 3 x 3 pixel matrix is considered as local offset [10].
2. The analysis of the local phase histogram provides the local offset. We assume that the noise is randomly distributed over all histogram entries, so that the largest histogram entry corresponds to less noisy phase values. Its mean value is therefore calculated to be the desired offset. If no histogram interval shows significant entry, the offset is set to zero.
3. Investigation of simulated InSAR phases for resolving the underestimation of the heights by extracting the local offset. It is necessary to have an initial building height, so that a building signature can be simulated.

The results from the coherence weighted mean filter [7] within a 5 x 5 pixel window are presented in Fig. 3 for the three introduced phase unwrapping approaches together with the result without any phase unwrapping. For each method, the corresponding offset image is given in the first row of Fig. 3. In Tab. 1, the standard deviation of the phase values and the correlation value between the filtered phase image and the simulated phase image are listed.

Table 1. Standard deviation and correlation values of filtered phases using different unwrapping methods

	Without	**Complex**	**Histogram**	**Simulation**
σ_{image} [rad]	0.29	0.67	0.40	0.28
ρ [0;1]	0.47	0.44	0.48	0.66

An underestimation of the filtered phase values is visible in (a), especially in the roof area. All three unwrapping methods resolve this problem given in (b), (c) and (d). The shadow region is better filtered by histogram (c) and simulation (d) based methods as by complex averaging (b) method. For the histogram method, this is due to an offset value of mainly zero in the shadow area caused by the assumption of significant histogram entries. Additionally, the simulation method delivers in the shadow region only the value zero since no shadow simulation is accomplished [13]. This approach delivers best results, especially by recovering sharp building edges, so that in the following, we prefer the histogram analysis only for initial phase filtering (no building height available for simulation) while simulated phases are used for a more accurate estimation.

3. TEST DATA

The described phase filters are applied on real InSAR data showing an industrial building with a size of approx. 60 m width and approx. 100 m length. The choice of single-pass InSAR data was driven by minimizing noise due to temporal decorrelation, since this kind of noise can be almost neglected for single-pass systems like TanDEM-X. We performed our tests with imagery of the airborne sensor Aes-1 ([14]). The system operated in X-band at 3000 m flight height with a spatial resolution of about 38 cm in range and 17 cm in azimuth direction. The baseline was about 2.4 m and the scene was illuminated with an off-nadir angle spanning a range from 28° up to 52°. In Fig. 4, the optical building signature, the GIS information as well as its InSAR signature in the magnitude, phase and coherence images

are shown. Differences in the phase signatures between the real data and the simulated data are only visible in the upper part of the shadow area due to a porch, which is not modelled, and in the layover area due to occlusion effects caused by closed trees. In the future the filtering of single-pass TanDEM-X data will be investigated.

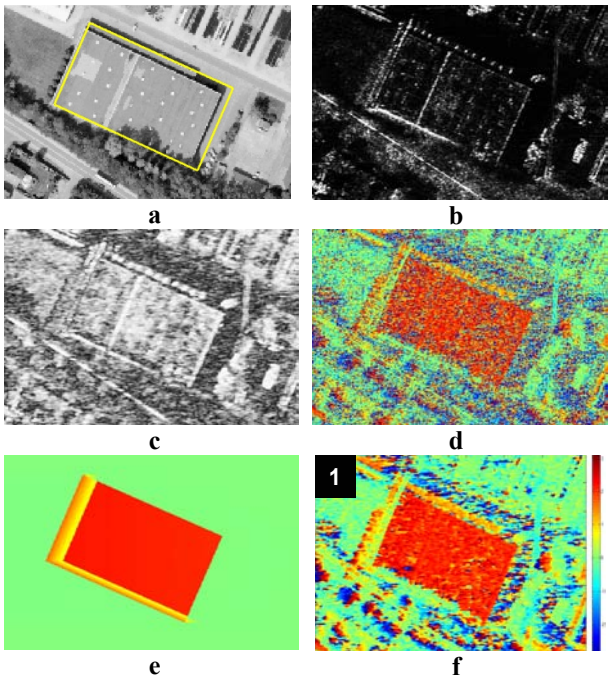

Figure 4. Test Data; a) aerial image with footprint, b) magnitude, c) coherence, d) phase, e) simulated phase, f) Multilook filtering 1*, window size: 5x5*

4. RESULTS

In the following, a visual analysis of filtered building phase signatures as well as a numerical assessment of the filter results is given. For the majority of filters we used a 5 x 5 pixel filter window to achieve comparable results. Moreover, the number of pixel in a 5 x 5 window is approximately the same as in an oriented 9 x 9 window, used by 8 – 11. Only for filtering in the frequency domain (2 – 5), we used a 25 x 25 window size, so that the pixel sample is big enough to distinguish high frequencies from low frequencies.

4.1. Visual Results

The visual results of Area Filters are presented for the Multilook-filter in Fig. 4 and for the others in Fig. 5. It is observable that the modified Goldstein and Baran filter (3 and 5) obviously provides a better smoothing than the standard methods (2 and 4). The results obtained by Goldstein filtering are slightly better than the Baran based. This is due to the smoothing parameter, which is fixed for Goldstein and coherence dependent for Baran. Seeing that the coherence at building roof is non-uniform, the smoothing effect is non-uniform neither. The coherence weighted mean filter 7 with simulation based phase unwrapping shows better results as the median filter 6. There is no underestimation of the building height anymore, and the edges are better preserved. Regarding the orientation filters, no important difference occurs between the standard Lee 8 and the modified Lee 9. For the GIS supported filters, the same remarks can be for median (10 and 12) and weighted

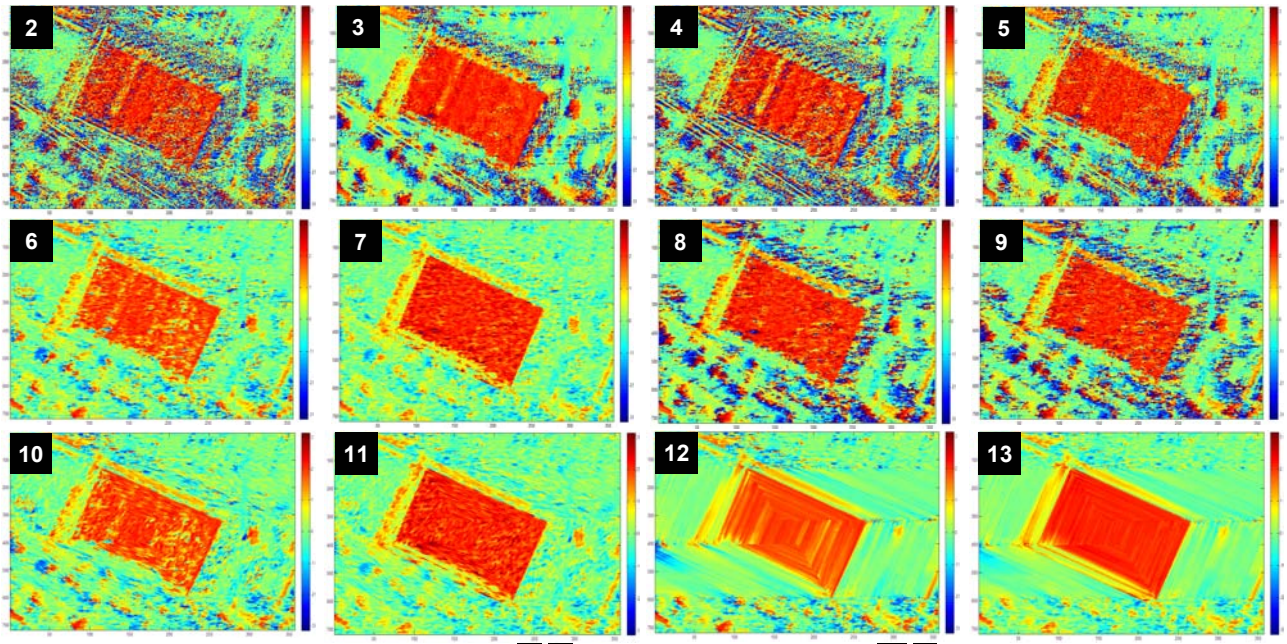

Figure 5. Filter results. Area filters: 2*,* 3 *window size=25x25, α=0.6,* 4*,* 5 *window size=25x25,* 6*,* 7 *window size=5x5.Orientation filters:* 8*,* 9 *window size=9x9. GIS supported filters:* 10*,* 11 *window size=9x9,* 12*,* 13 *window size: adaptive*

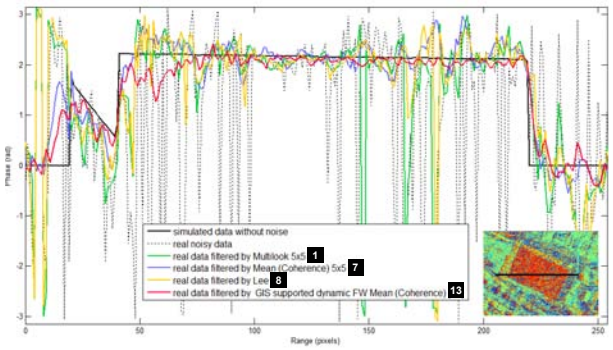

Figure 6. Slant-Range Phase Profiles

mean filter (11 and 13) as for the area filter. In comparison to the other filters with fixed window size (10 and 11), the adaptive GIS supported filters (12 and 13) provide obviously better results. The edges are very good preserved, especially the layover is better reconstructed and the smoothing in the roof is uniform.
Phase profiles from four of the presented filters are illustrated in Fig. 6 overlaid with real and simulated phase profiles. The profile of the new adaptive GIS supported filter (red coloured) is the closest to the simulated profile (black coloured).

4.2. Numerical Results

The numerical validation of our filter results is based on four different evaluation parameters.

1. The mean local standard deviation of filtered phases defined by

$$\sigma_{\text{image}} = \frac{\sum_{i=1}^{m}\left(\frac{1}{n-1}\sum_{j=1}^{n}(\Delta\varphi_j - \overline{\Delta\varphi})^2\right)^{1/2}}{m}$$

   where n=25 (local window of 5 x 5 pixels) and m is the number of pixels in the whole image.

2. The mean difference μ_{diff} between simulated and filtered phase images.

3. The standard deviation of differences σ_{diff} between simulated and filtered phase images.

4. The cross correlation ρ between filtered and noise-free simulated phases.

The three last values refer only to the building location (layover and roof area), so that the not simulated objects around the building do not affect the values.
The resulting evaluation parameters are summarized for all investigated filters in Tab. 2. From the group of area filters, the coherence weighted filter 7 shows best results, and the modified Goldstein and Baran filters (3 and 5) show an improvement in comparison to the standard filters (2 and 4). For the group of orientation filters, the modified Lee filter 9 delivers similar results to the standard Lee-filter 8. An improvement is visible by investigating building orientation from GIS with the same fixed windows size (10 and 11). The biggest improvement is shown for the adaptive GIS supported filter with coherence weighted mean 13. For this filter, a correlation value of 0.78 is achieved.

5. CONCLUSION AND OUTLOOK

In this paper, we presented several modified and enhanced filter approaches to smooth the interferometric phase image at building location. The incorporation of GIS information like the building footprint allows considering the exact edge direction and length of the building, so that adaptive filter windows can be defined for each pixel. Filter approaches combining these GIS information with a coherence-weighted mean filtering, showed best results. Of course, the geometric quality of the GIS data largely influences the efficiency of this approach. Additionally, different unwrapping methods were tested, whereby the integration of simulated phases as offset values preserved edges better as the other methods. Nevertheless, the histogram method can be applied in case of no available GIS information. In the future, it is envisaged that both unwrapping methods are combined to determinate first an initial building height based on a histogram supported filter result, which could be used in a second step for the simulation.
The results of the different filters were presented on real InSAR data recorded by a single-pass airborne SAR sensor. The visual and numerical interpretation confirmed the high potential of the new adaptive GIS supported filters, especially for applications of building reconstruction.
Further work will focus on additional tests considering different airborne and spaceborne InSAR data, especially the filtering of single-pass TanDEM-X data will

Table 2. Numerical Validation of Filtering Results

	org	1	2	3	4	5	6	7	8	9	10	11	12	13
σ_{image} [rad]	1.36	0.55	1.08	0.70	1.18	0.86	0.36	0.28	0.70	0.80	0.37	0.29	0.23	0.19
μ_{diff} [rad]	0.18	0.30	0.18	0.30	0.18	0.28	0.61	0.20	0.27	0.26	0.62	0.20	0.59	0.20
σ_{diff} [rad]	1.26	0.8	1.05	0.80	1.10	0.88	0.77	0.49	0.84	0.88	0.74	0.48	0.56	0.36
ρ [0;1]	0.19	0.50	0.31	0.49	0.27	0.41	0.50	0.66	0.45	0.41	0.51	0.68	0.62	0.78

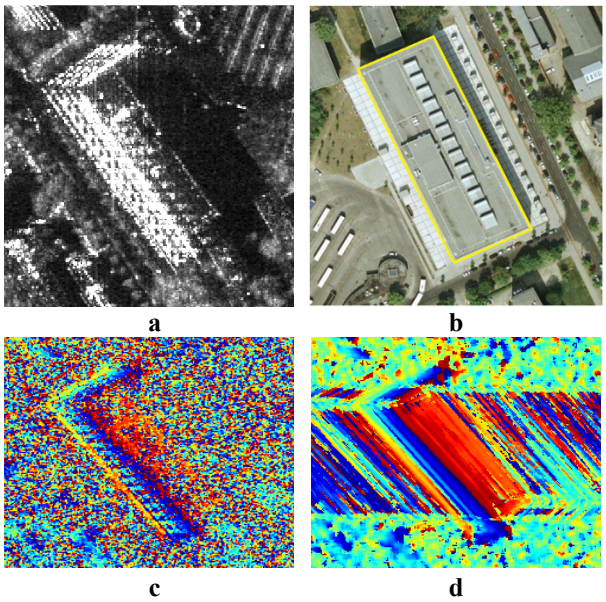

Figure 7. Outlook for satellite data: TerraSAR-X; a) coherence, b) aerial image, c) phase, d) phase filtered with adaptive GIS, coherence weighted mean

be investigated. A promising outlook is already given in Fig. 7 for a repeat-pass image pair of TerraSAR-X.
An adaptive method is planned to filter especially large buildings, whereby adaptive GIS filters for the layover area and area filter for the roof could be combined to enable improved filter results in these areas. In addition, other building models like gable-roofed buildings have to be considered, so that an appropriate filtering could be accomplished. Further, investigations on building neighbourhood should be mentioned here, because interaction effects between buildings can probably require an adaptation of phase filtering.

REFERENCES

[1] Thiele, A., Hinz, S., Cadario, E., 2010 Fusion of InSAR and GIS data for 3D building reconstruction and change detection. Proceedings of 'Fringe 2009 Workshop', Frascati, Italy, ESA SP-677, http://earth.eo.esa.int/workshops/fringe09/.

[2] Goldstein, R. M., Werner C. L., 1998 Radar interferogram filtering for geophysical applications. Geophysical Research Letters, vol. 25, no. 21, pp. 4035-4038.

[3] Baran, I., Stewart, M. P., Kampes, B. M., Perski, Z., Lilly P., 2003 A Modification to the Goldstein Radar Interferogram Filter. IEEE Transactions on Geoscience and Remote Sensing, vol. 41, no. 9, pp. 2114-2118.

[4] Tupin, F., 2011 How Advanced Image Processing Helps For SAR Image Restoration and Analysis. IEEE Geoscience and Remote Sensing Newsletter, Cumulative Issue 158, March 2011, ISSN: 0274-6338, pp. 10-17.

[5] Goldstein, R. M., Zebker, H. A., Werner, C. L., 1988 Satellite radar interferometry: Two-dimensional phase unwrapping. Radio Science, vol. 23, no. 4, pp. 713-720.

[6] Reeves, B., Homer, J., Stickley, G., Noon, D., Longstaff, I.D., 1999 Spatial vector filtering to reduce noise in interferometric phase images. IEEE International Geoscience and Remote Sensing Symposium (IGARSS), doi: 10.1109/IGARSS.1999.773465, vol. 1, pp. 260-263.

[7] López-Martínez, C., Fàbregas, and X., 2002 Modeling and reduction of SAR interferometric phase noise in the wavelet domain. IEEE Transactions on Geoscience and Remote Sensing, vol. 40, no. 12, pp. 2553–2566..

[8] Ciuc, M., Trouve, E., Bolon, P., Buzuloiu, V., 2002 Amplitude-driven coherence filtering in complex interferograms. IEEE International Geoscience and Remote Sensing Symposium (IGARSS), doi: 10.1109/IGARSS.2002.1027213, vol. 6, pp. 3453-3455.

[9] Vasile, G., Emmanuel, T., 2004 General adaptive neighborhood technique for improving synthetic aperture radar interferometric coherence estimation. Journal of the Optical Society of America A, vol. 21, no. 8, pp. 1455-1464.

[10] Lee, J.-S., Papathanassiou, K. P., Ainsworth, T. L., Grunes, M. R., Reigber, A., 1998 A new technique for noise filtering of SAR interferometric phase images. IEEE Transactions on Geoscience and Remote Sensing, vol. 36, no. 5, pp. 1456-1465.

[11] Bo, G., Dellepiane, S., Beneventano, G., 1999 A locally adaptive approach for interferometric phase noise reduction. IEEE International Geoscience and Remote Sensing Symposium (IGARSS), doi: 10.1109/IGARSS.1999.773466, vol. 1, pp. 264-266.

[12] Rejichi, S., Chaabane, F., Tupin, F., Bloch, I., 2010 Morphological filtering of SAR interferometric images. IEEE International Geoscience and Remote Sensing Symposium (IGARSS), doi: 10.1109/IGARSS.2010.5653767, pp. 1581-1584.

[13] Thiele, A., Cadario, E., Schulz, K., Thoennessen, U., Soergel, U., 2007 InSAR Phase Profiles at Building Locations. Proceeding of ISPRS Photogrammetric Image Analysis, vol. XXXVI, part 3/W49A, pp. 203-208.

[14] Schwaebisch, M., Moreira, J., 1999 The high resolution airborne interferometric SAR AeS-1. Proceedings of the Fourth International Airborne Remote Sensing Conference and Exhibition, Canada, pp. 540-547.